Hydrothermal assisted synthesis followed by reduction route: $Gd_2O_2S:Eu^{3+}$ hollow spheres and their photoluminescence properties

HUILIN QU, JINGBAO LIAN*, HUA QIN, NIANCHU WU, XUE ZHANG, JIAO HE
School of Mechanical Engineering, Liaoning Petrochemical University, Fushun, 113001, P.R. China

Herein, a homogeneous $Gd_2O_2S:Eu^{3+}$ hollow spheres with pure phase structure were synthesized successfully through the calcination and reduction of the precursors prepared by hydrothermal method. It's worth noting that the non-template method is used to replace the traditional template method in this paper. The optimum calcination temperature of the precursor is 800 ^oC. FE-SEM and TEM observation indicate the target products are hollow spheres with a size range of 200-400 nm. When the doping concentration of Eu^{3+} is 7.50%, the luminescence intensity is the highest and its CIE coordinate fluorescence lifetime are (0.629, 0.370) and 1.114 μs.

(Received January 11, 2022; accepted August 10, 2022)

Keywords: Rare earth luminescent materials, Gadolinium oxysulfide, Hollow spheres, Reduction route, Photoluminescence

1. Introduction

It's universally acknowledge that there exists several mainly ways to light up: photoluminescence, electroluminescence, cathodoluminescence, X-ray luminescence and high energy particle luminescence, etc. Rare earth luminescent materials exhibit a wide band gap and excellent luminescence properties arising from their intra 4f transitions, large anti-stokes shifts and stokes shifts (up to 500 nm) [1,2]. Then they have been widely used in several of areas, like biomarker, military, nuclear physics, radiation and so on [3]. Especially, rare earth ions activated gadolinium oxysulfide (Gd_2O_2S) has advantage of high light absorption, high energy transfer efficiency, high X-ray blocking ability, short attenuation time, good irradiation stability and good scintillation properties [4-8]. Therefore, they make contribution in plasma display panel, X-ray phosphor, X-CT, positron emission computed tomography (PET), medical radiotherapy linear accelerator and so on [9].

In recent years, rare earth luminescent materials with micro and nano hollow structure have arose far-reaching attention [10], so that it can contain a large number of guest molecules or large-size guest molecules [11]. Because of its high surface activity and good surface permeability [12], hollow sphere is widely used in drug release, magnetic storage materials, dye precipitation and catalytic applications [13]. For instance, a magnetic core can be covered with a porous silica shell that can be loaded with drugs and provide biocompatibility [14]. From this point of view, no matter in terms of radiation efficiency, decay time, chemical stability or radiation damage resistance, Gd_2O_2S is a good host matrix suitable for doping rare earth ions to fabricate phosphors [15]. Gd_2O_2S activated by trivalent europium ions ($Gd_2O_2S:Eu^{3+}$) can effectively improve the luminescent center and make them become important red phosphors [16].

To our best knowledge, a flawless preparation method has rarely been reported, so we need to work hard to develop new methods. Conventionally, a variety of strategies have been adopted for the design and synthesis of hollow spheres, including template method [17], microemulsion method [18], electrospinning method [19] and hydrothermal/solvothermal method [20]. Template method can be divided into soft template method and hard template method. Nevertheless, this preparation method is gradually replaced by other preparation methods because of its easy condensation, complicated steps, low yield and high cost. In the traditional sense, due to the existence of sulfur, the nano particles prepared by microemulsion method have irregular morphology, and the powder is easy to be destroyed. The product prepared by electrospinning has the characteristics of good solubility, high flexibility, non-toxic, easy preparation and low cost. While the morphology of the product is affected by the experimental conditions, which also has some limitations. Hydrothermal/solvothermal method can make hollow spheres with high purity, complete crystal growth and narrow particle size distribution, which means that the agglomeration degree of particles is light and energy consumption is low, while there is still exist a little defect compared with the method this paper involves.

In consideration of the limitations of various methods, we first proposed to prepare $Gd_2O_2S:Eu^{3+}$ hollow spheres through hydrothermal assisted synthesis followed by reduction route. Furthermore, the obtained samples were characterized systematically by XRD, DSC-TG, FT-IR, FE-SEM, TEM and PL. Compared with the traditional template synthesis, this synthesis route is one of the optimal method because it is easy to operate and put into production without pollution. Moreover, this synthesis route is economical, environmental friendly, and free from using toxic CS_2, H_2S or sulfur vapor in the synthesis process.

2. Experimental procedure

2.1. Synthesis

Gadolinium nitrate hexahydrate ($Gd(NO_3)_3·6H_2O$), Europium nitrate hexahydrate ($Eu(NO_3)_3·6H_2O$), ammonia ($NH_3·H_2O$), L-cysteine ($C_3H_7NO_2S$) and PVP-K30 ($(C_6H_9NO)_n$) were used as the starting materials without further purification. $Gd(NO_3)_3·6H_2O$ and $Eu(NO_3)_3·6H_2O$ were purchased from Jining Tianyi New Material Co. Ltd, China. The other reagents were purchased from Sinopharm Chemical Reagent Co. Ltd, China. Firstly, $Gd(NO_3)_3·6H_2O$ and $Eu(NO_3)_3·6H_2O$ salts were dissolved in deionized water to obtain 0.04 $mol·L^{-1}$ $Gd(NO_3)_3$ and $Eu(NO_3)_3$ solutions, respectively, and the pH values of two solutions were adjusted with $NH_3·H_2O$. Secondly, $Gd(NO_3)_3$ solution with volume of 50 mL was transferred to a 100 mL Teflon-lined stainless steel autoclave. Accompanied with stirring, a certain amount of L-cysteine was added to $Gd(NO_3)_3$ solution until it was completely dissolved. Then 0 g, 0.3 g and 0.6 g PVP were also added to the autoclaves, respectively. After PVP was completely dissolved, the autoclaves were sealed and heated in an electric blast drying oven for hydrothermal synthesis at 140 °C for different time (6-24 h). When the autoclaves was cooled to room temperature, the yellow precipitate was washed several times with deionized water and absolute ethanol, and dried at 80 °C for several hours to obtain the precursor. The Eu^{3+} ion-doped precursors were also synthesized using the same procedure. The precursors were calcined at 800 °C for 2 h in a high temperature box resistance furnace to obtain the intermediate products. Finally, the intermediate products were reduced at 600 °C for 2 h in a mixture of flowing argon and hydrogen (90% Ar+10% H_2) to form the target products, Gd_2O_2S. When the precursors doped with Eu^{3+} were calcined and reduced, $Gd_2O_2S:Eu^{3+}$ hollow spheres can be obtained. The experimental flow chart is shown in Fig. 1.

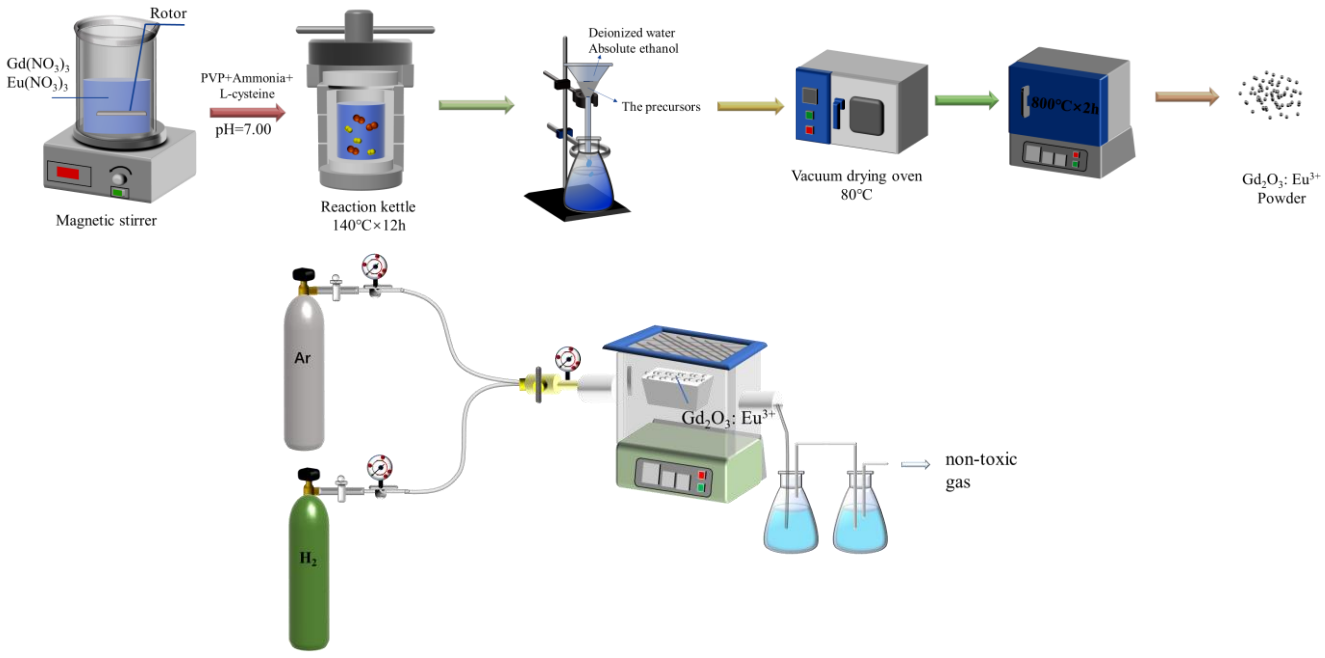

Fig. 1. Schematic illustration for the synthesis of $Gd_2O_2S:Eu^{3+}$ hollow spheres (color online)

2.2. Characterization

X-ray diffraction (XRD) analyses were carried out using a D8 Advance X-Ray diffractometer with Cu Kα radiation (λ=0.15406 nm). And its working voltage is 40 kV, working current is 30 mA, 2θ value from 10° to 90° when collect the data. The particle morphologies of the products were obtained by a Hitachi SU8000 field emission scanning electron microscopy (FE-SEM) at the accelerating voltage of 15.0 kV. And the hollow structure areas and surface mapping were observed by a JEOL-2100 transmission electron microscopy (TEM) equipped with

EDX. The structure of the synthesized product was analyzed by FT-IR with an Agilent Cary 660. The KBr method was used in the wave number range of 4000-400 cm^{-1}. The thermogravimetry and differential scanning calorimetry (TG-DSC) curves were measured by PerkinElmer SDT 2960 simultaneous DSC-TGA thermal analyzer in a temperature range of 25-1400 °C at a heating rate of 5 $^{o}C \cdot min^{-1}$ under an air flow. The photoluminescence (PL) spectra and decay time of the final product were measured by Hitachi F-4600 fluorescence spectrophotometer equipped IBH TemPro fluorescence lifetime measurement system.

3. Results and discussion

3.1. Selection of optimal pH value

In order to obtain a pure product with high yield, it is very necessary to adjust the pH value of the initial solution. By titrating a certain amount of ammonia into the initial $Gd(NO_3)_3$ solution with pH=5.14, the pH values of the other two solutions was adjusted to 7.00 and 7.20 in this work. Then the precursors synthesized with three different pH values were calcined at 800 ^{o}C for 2 h in air, and the XRD phase analysis was carried out. Fig. 2 shows XRD patterns of the calcination products with various pH values and the standard data of $Gd_2O_2SO_4$ with JCPDS card No.00-41-0683 for comparison. As shown in Fig. 2(a), when the pH value of the system is not adjusted by ammonia water, that is pH=5.14, the XRD pattern shows obvious sharp diffraction peaks, indicating that it has good crystallinity. Comparing all the diffraction peaks with the JCPDS card (00-41-0683) of $Gd_2O_2SO_4$ in Fig. 2(d), it is found that the diffraction peaks of both are in good agreement. It is confirmed that when pH=5.14, the calcination product is pure $Gd_2O_2SO_4$ phase. When the pH value of $Gd(NO_3)_3$ solution amounts to 7.00, it can be seen from Fig. 2(b) that the XRD pattern has no obvious change compared with Fig. 2(a), indicating that the calcined product is still pure $Gd_2O_2SO_4$ phase at pH=7.00. However, we found that the yield of the precursor was higher when pH=7.00. When the pH value of $Gd(NO_3)_3$ solution is 7.20, it can be seen from Fig. 2(c) that a weak diffraction peak near 2θ=18.51° appears, which is not belong to $Gd_2O_2SO_4$ phase, that is, the impurity phase appears in the product and the purity decreases. In conclusion, the above XRD pattern analysis shows that the precursor synthesized at pH=7.00 can synthesize pure $Gd_2O_2SO_4$ phase, and the yield of calcined product is high. Therefore, the following discussion in this work is based on the precursor synthesized at pH=7.00 and its calcined product.

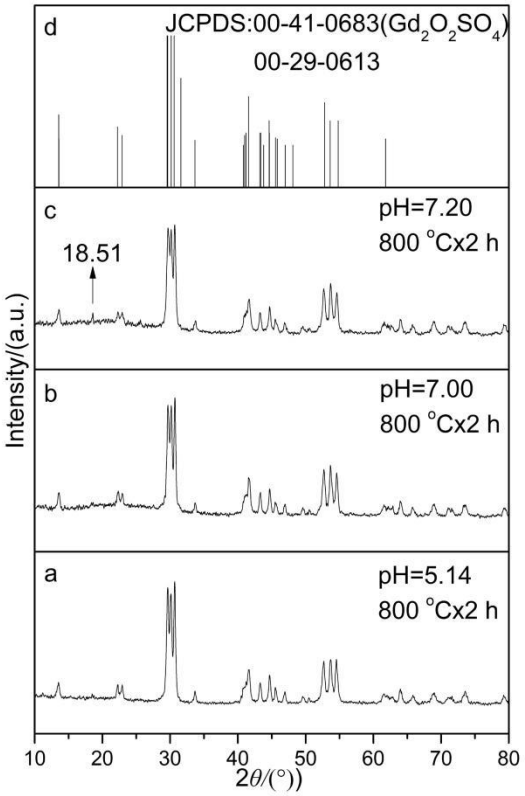

Fig. 2. X-ray diffraction patterns of the as-obtained products with various pH: (a) pH=5.14; (b) pH=7.00; (c) pH=7.20; The pattern of (d) is the data of $Gd_2O_2SO_4$ with JCPDS card No.00-41-0683 for comparison

3.2. Thermal conversion process

The key step for the formation of pure $Gd_2O_2SO_4$ is the thermally driven decomposition of the precursor prepared by hydrothermal synthesis. Therefore, it is very important to understand the thermal decomposition process of precursor for obtaining pure $Gd_2O_2SO_4$. TG-DSC were used to determine the thermal decomposition process of the precursor, as shown in Fig. 3.

When the temperature was between room temperature and 1400 ^{o}C, the precursor lost weight continuously, and the total mass decreased by 56.08%. Three steps of weight loss are observed in TG curves of the precursor. The first gradual weight loss between room temperature and 580 ^{o}C is attributed to the gradual evaporation of adsorbed water and the oxidization of combustion organic functional groups in the precursor with the weight loss rate of 43.79%. Accordingly, this weight loss corresponds to a very weak endothermic peak at around 64 ^{o}C and a strong and broad exothermic peak centered at 358 ^{o}C. The second gentle weight loss in the temperature range of 580 ^{o}C to 970 ^{o}C may belong to the decomposition process of carboxyl in the precursor with the weight loss rate of 5.28%. There was no obvious endothermic or exothermic peaks in the DSC curve. The third weight loss with slow

down speed in the temperature range of 970 °C to 1400 °C is concerned with the high temperature thermal decomposition of $Gd_2O_2SO_4$ with the weight loss rate of 7.01%. Accordingly, two endothermic peaks centered at 1016 °C and 1137 °C appear in DSC curve, corresponding to the following chemical reaction equation [(1)]:

$$Gd_2O_2SO_4=Gd_2O_3+SO_2\uparrow+1/2O_2\uparrow \quad (1)$$

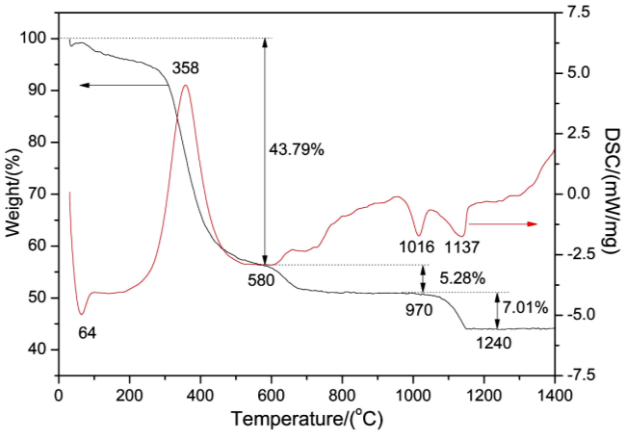

Fig. 3. TG-DSC curves of precursors in air between room temperature and 1400 °C (color online)

The TG curve between 700 °C and 970 °C is approximately straight, and the precursor has constant weight, which can be used as a temperature window for the synthesis of pure $Gd_2O_2SO_4$. In this experiment, 800 °C was selected as the best calcination temperature for the intermediate product ($Gd_2O_2SO_4$) in order to ensure that the synthesized product has a certain crystallinity and can not decompose into heterophase.

3.3. Phase analysis of target product

Fig. 4 shows the XRD patterns of $Gd_2O_2SO_4$ calcined at 600 °C for 2 h in Ar and hydrogen atmosphere and the standard card of JCPDS card (00-26-1422) of Gd_2O_2S. It can be observed from Fig. 4a that the XRD pattern presents some obvious diffraction peaks, indicating that the reduction product crystallizes well. The well-defined diffraction peaks can be readily indexed to the standard pattern of Gd_2O_2S (JCPDS No.00-26-1422), as shown in Fig. 4b, which further confirmed that the $Gd_2O_2SO_4$ can be transformed into the Gd_2O_2S in reducing atmosphere. The chemical reaction equation is as follows:

$$Gd_2O_2SO_4+4H_2=Gd_2O_2S+4H_2O\uparrow \quad (2)$$

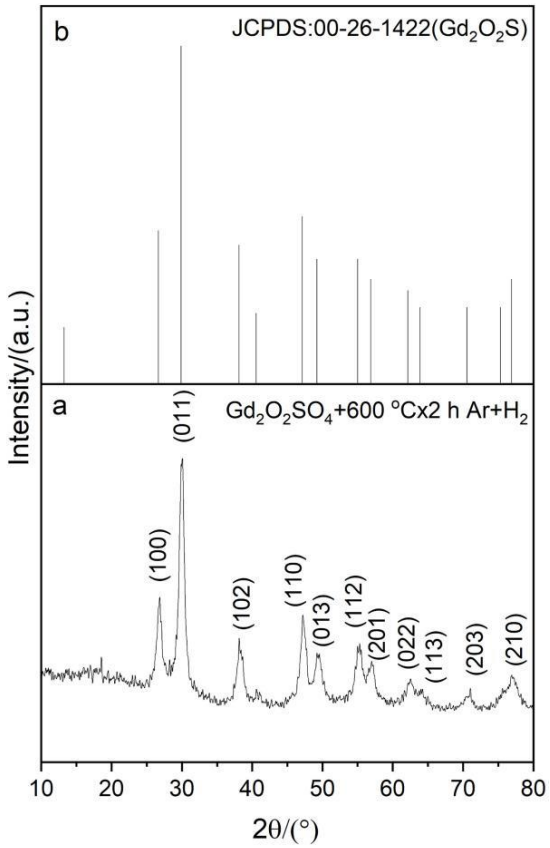

Fig. 4. XRD patterns of $Gd_2O_2SO_4$ calcined at 600 °C for 2 h in reducing atmosphere

3.4. FT-IR spectra of the synthetic products

The functional groups were studied by FT-IR. Fig. 5 shows the infrared absorption spectra of the precursor, the $Gd_2O_2SO_4$ and the Gd_2O_2S. In Fig. 5a, the strong absorption peak at 3430 cm^{-1} is attributed to the stretching peak of water molecules in the precursor, indicating the existence of adsorbed water in the precursor. The 2925 cm^{-1} absorption peak may be related to the presence of CO_2 in the test environment. While the -SH group vibration (2550-2750 cm^{-1}) is absent on the surface, indicating that the -SH group was bound to the matrix to form a covalent bond, providing evidence for the binding of L-cysteine to surface particles. The -COOH characteristic peaks is located at between 1285-1670 cm^{-1}, which is the coordination carboxyl vibration. The absorption peak of C-S bond is observed near 670 cm^{-1}, which provides the sulfur source of the $Gd_2O_2SO_4$.

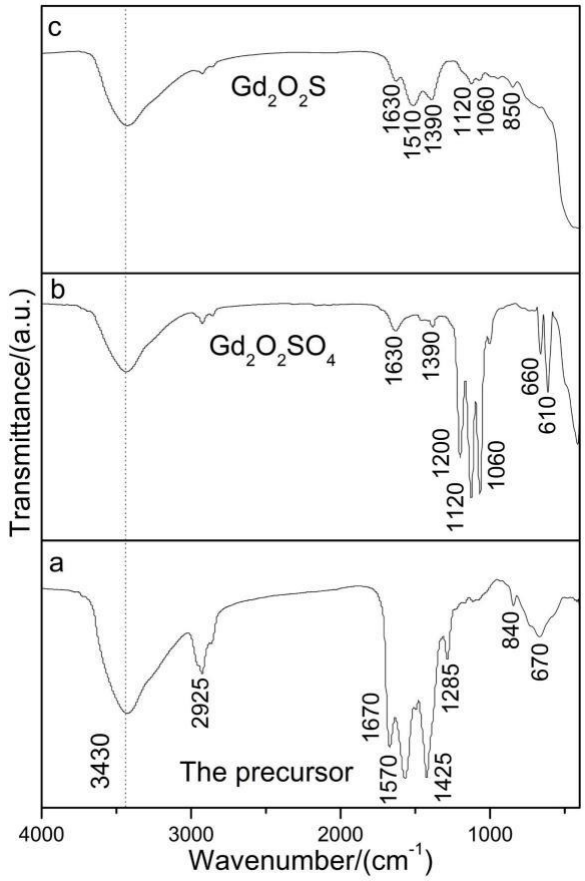

Fig. 5. FT-IR analysis of the precursor, the $Gd_2O_2SO_4$ and the Gd_2O_2S

When the precursor was calcined at 800 ^oC for 2 h in air, it is seen from Fig. 5b that the splitting absorption peaks of SO_4^{2-} were observed at 1200 cm^{-1}, 1060 cm^{-1}, 1120 cm^{-1} and 660 cm^{-1}, 610 cm^{-1}. Moreover, the absorption peaks at 3430 cm^{-1} and 1630 cm^{-1} indicate the existence of adsorbed water in the $Gd_2O_2SO_4$. The infrared spectrum of the target product Gd_2O_2S (Fig. 5c) still has a weak absorption peak near 3430 cm^{-1}, 1630 cm^{-1}, 1510 cm^{-1}, 1390 cm^{-1}, 1120 cm^{-1}, 1060 cm^{-1}, 850 cm^{-1}, indicating that the Gd_2O_2S is also easy to absorb water and carbon dioxide in the air.

3.5. Morphology analysis of the synthetic products

Fig. 6 shows FE-SEM images of the precursor synthesized under the condition of fixed amount of PVP=0.3 g and different hydrothermal reaction time (6 h, 12 h, 24 h). In Fig. 6a, the precursor exhibits relatively narrow size distribution with 200-400 nm in diameter and poor dispersion without hollow structure areas. When the hydrothermal synthesis time is 12 h, it is concluded from Fig. 6b that the precursor is quasi spherical in shape, uniform and hollow structure can be observed. The particle size range is between 300 nm and 400 nm. In addition, the dispersivity is not changed obviously, and the agglomeration phenomenon is still present. When the hydrothermal synthesis time is 24 h, although the Fig. 6c shows the synthesized precursor has hollow structure with small size, while accompanied by waste of energy resources and low productivity. Therefore, we finally choose the optimal hydrothermal time of 12 h in the study.

In the process of hydrothermal reaction, PVP was coated on the surface of the particles as a surfactant to form a protective layer to control the size and growth rate of the precursor particles. PVP solution with high enough concentration can be completely wrapped in all directions of the precursor particle surface to ensure the isotropic growth of the precursor, so as to obtain stable microspheres. Therefore, the size of spherical particles is generally controlled by changing its content. Fig. 7 shows FE-SEM images of Gd_2O_2S synthesized at 140℃ for 12 h with different PVP contents. In Fig. 7a, when PVP is 0 g, the product particles have a near spherical structure, and the particle size is about 3 μm. There are many 500 nm balls distributed on the surface of the spherical particles, and the agglomeration phenomenon occurs. From Fig. 7b, when PVP amounts to 0.3 g, it can be seen the morphology of the product has changed significantly, it no longer has the characteristics of villous structure, the product becomes nearly spherical and its diameter is about 200 nm, which still has the characteristics of aggregate and the dispersion is general but the hollow feature is obvious with smooth surfaces. With the increase of PVP content to 0.6 g, it can be seen from Fig. 7c that the size of the product decreases, many spherical particles are less than 200 nm in diameter, and the agglomeration phenomenon can not be eliminated, the surface of hollow spheres became relatively rough. As the reasonable amount for synthesizing hollow spherical structure in this study. In conclusion, the addition of PVP is necessary to obtain hollow structure. In order to save the amount of PVP, 0.3 g PVP was selected as the reasonable amount for synthesizing hollow spherical structure in this study.

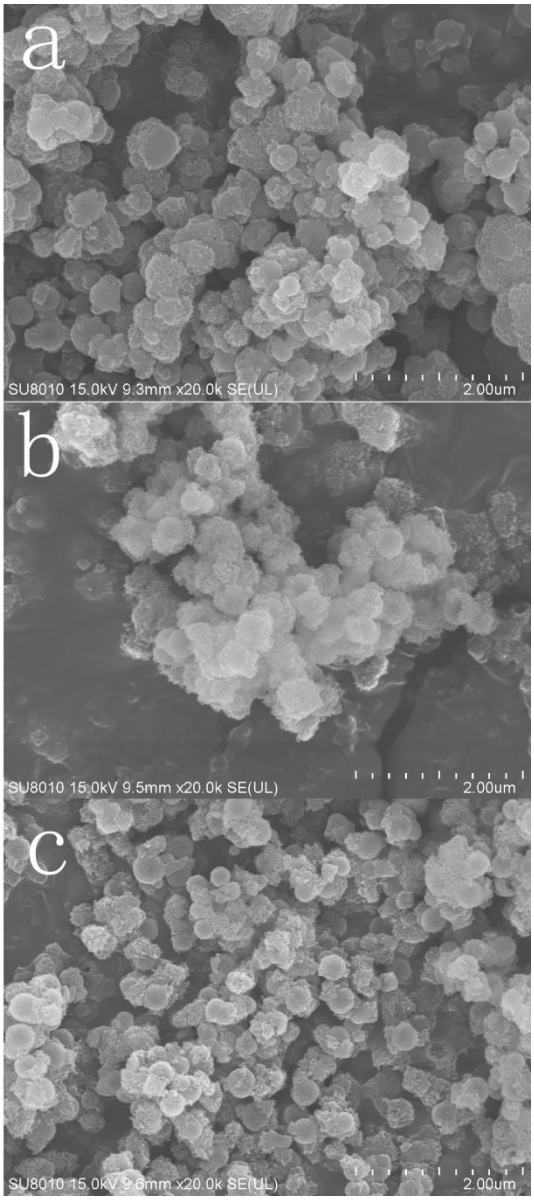

Fig. 6. FE-SEM images of precursors at different hydrothermal time (a) 6 h; (b) 12 h; (c) 24 h

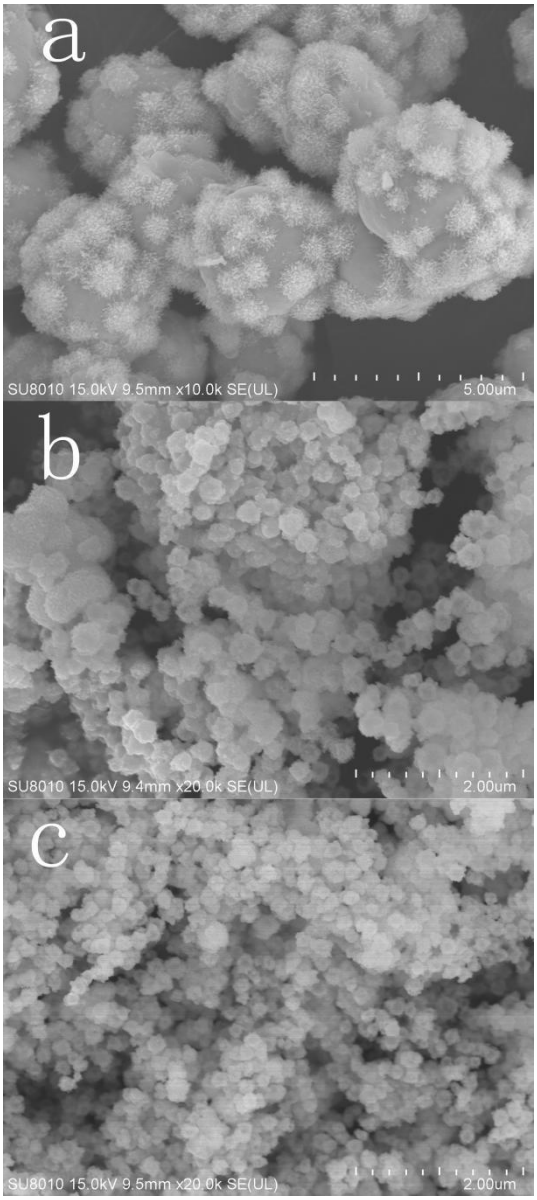

Fig. 7. FE-SEM images of Gd_2O_2S synthesized with different PVP contents (a) 0g; (b) 0.3g; (c) 0.6g

In order to further confirm the hollow spherical characteristics of the synthesized products, TEM analysis was carried out. It can be seen from Fig. 8a that the strongly contrast between the dark periphery and greyish center of the precursor reveals that these spheres with good dispersion were of hollow structures, and the shell thickness was about 50 nm, which the size of the precursor is about 300 nm-400 nm. After calcined the precursor at 800 ^oC for 2 h in air, it can be seen from Fig. 8b that the particle size of the $Gd_2O_2SO_4$ is about 200 nm, which is smaller than that of the precursor. It's may be related to the size shrinkage caused by the removal of organic functional groups in the precursor at high temperature. What's more, the hollow structure is still obvious and the dispersion is good. When the $Gd_2O_2SO_4$ was calcined at 600 ^oC for 2 h in the reducing atmosphere, it can be seen from Fig. 8c that based on the heredity of the morphology of the $Gd_2O_2SO_4$, the obtained Gd_2O_2S is still hollow spherical structure with a diameter of about 200 nm, which is consistent with the FE-SEM observation in Fig. 7c, and the dispersion is still good.

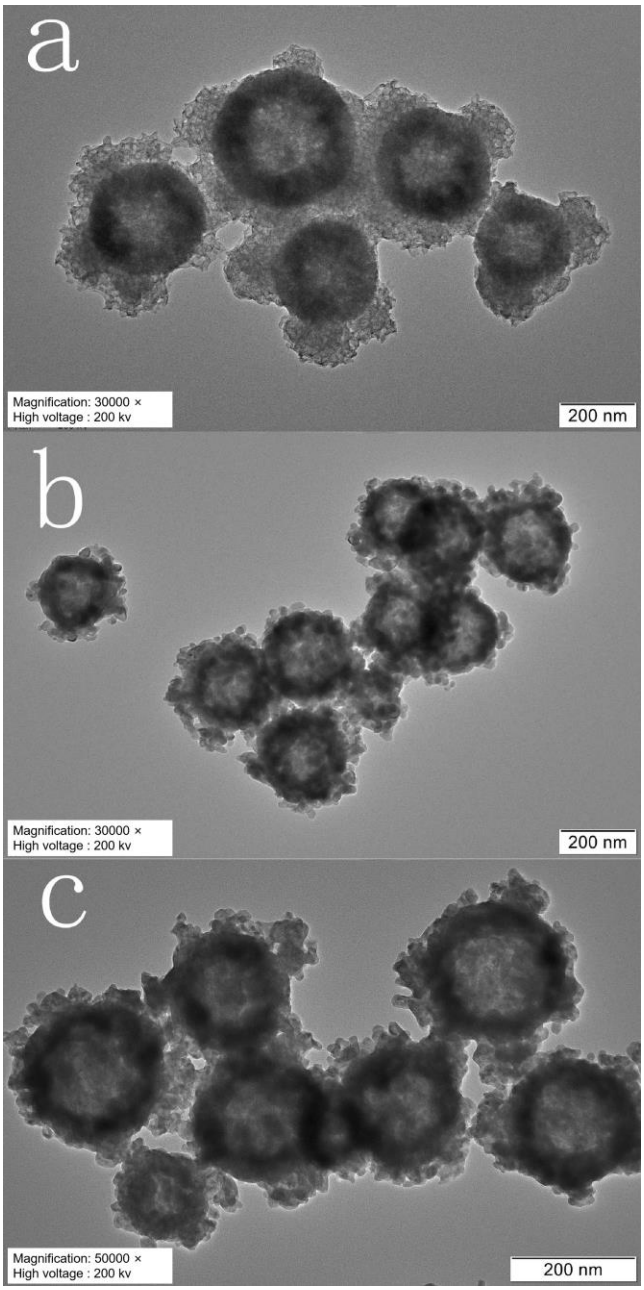

Fig. 8. TEM images of (a) the precursor, (b) $Gd_2O_2SO_4$ and the Gd_2O_2S

Fig. 9 shows the surface scan images of the target product Gd_2O_2S, which clearly demonstrates a homogeneous distribution of the target product are composed of Gd, O and S elements, and the distribution of Gd, O and S is uniform. These results further confirm that the host lattice structure is composed of Gd_2O_2S. What's more, it's consistent with the XRD pattern of the target product obtained by calcining at 600 ^oC for 2 h in $Gd_2O_2SO_4$ reduction atmosphere in Fig. 4.

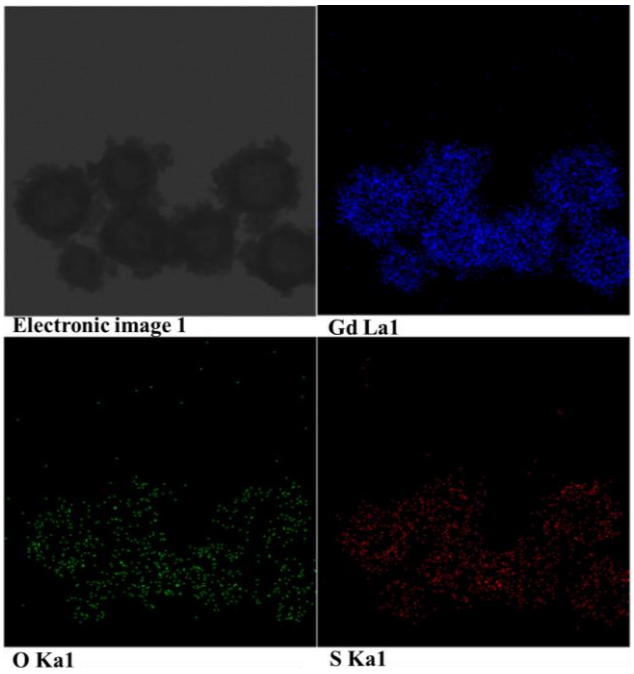

Fig. 9. The surface scan images of the Gd_2O_2S (color online)

3.6. Hollow structure formation mechanism of the Gd_2O_2S

In this work, the precursor was prepared using a hydrothermal method, where PVP and L-cysteine are dissolved in the $Gd(NO_3)_3$ solution. Herein, we have a bold guess about the formation of the hollow sphere. In the starting stage, L-cysteine as sulfur source plays a major reaction role and tends to coordinate with inorganic cations [21]. L-cysteine ions react with rare earth ions to form complexes. Then free L-cysteine is attached to the surface of the sphere. After PVP was added, PVP plays an important role as the surface modifier to control the size and agglomeration of spheres [22]. PVP molecules react with hydrogen bonds of the precursor, and C═O coordinates with unsaturated metal atoms of ions in the precursor. Through the self aggregation behavior of PVP, the growth of the grain can be prohibited and small-size particles are rapidly formed under high saturation conditions. After self-assembly, the outermost surface is aggregated under low saturation conditions, and the binding force with L-cysteine is increased, resulting in small intermediate particles and poor crystallinity, forming hollow spheres. The intermediate products obtained by calcination in air and the Gd_2O_2S powder reduced by argon and hydrogen still show the morphology of hollow spheres. The formation process is shown in Fig. 10.

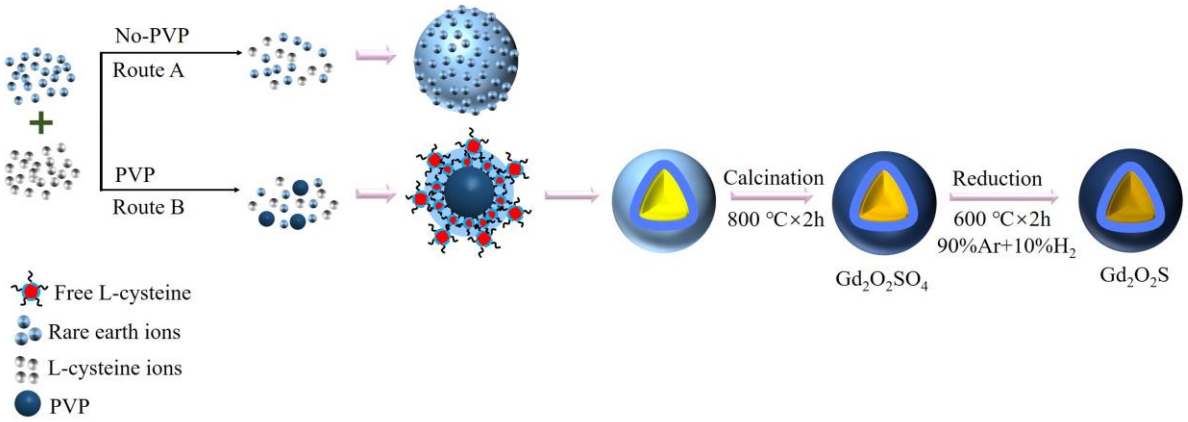

Fig. 10. Schematic formation process of the Gd_2O_2S hollow spheres (color online)

3.7. Photoluminescence properties

Fig. 11 shows the excitation and emission spectra of Gd_2O_2S:7.5%Eu^{3+} hollow spheres. In Fig. 11a, in the longer wavelength region, it is observed that the weaker and sharper f-f transition peaks of the Eu^{3+} ions (395 nm, 465 nm). The strong and broad excitation band ranging from 200 to 270 nm are ascribed to the matrix lattice absorption from Gd_2O_2S, we can prove by formula:

$$E_g=1240/\lambda(eV) \quad (3)$$

when λ=270 nm, E_g=4.593 eV. The one around 395 nm is attributed to $^7F_0 \rightarrow {}^5D_6$ transition of Eu^{3+} ions, and the other around 465 nm is attributed to $^7F_0 \rightarrow {}^5D_2$ transition of Eu^{3+} ions. The emission spectrum of Gd_2O_2S:7.5%Eu^{3+} hollow sphere is shown in Fig. 11b. Upon excitation at 465 nm of blue light, there are two broad emission bands in the range of 550 nm-650 nm. The strongest emission band is found at 626 nm, which is attributed to $^5D_0 \rightarrow {}^7F_2$ transition of Eu^{3+} ions. In addition, a weak emission band appears at 595 nm is attributed to the $^5D_0 \rightarrow {}^7F_1$ transition of Eu^{3+} ions. This is normally associated with Eu^{3+} cations occupying crystallographic sites, which is exist with the displacement of Gd^{3+} by Eu^{3+} ions [23].

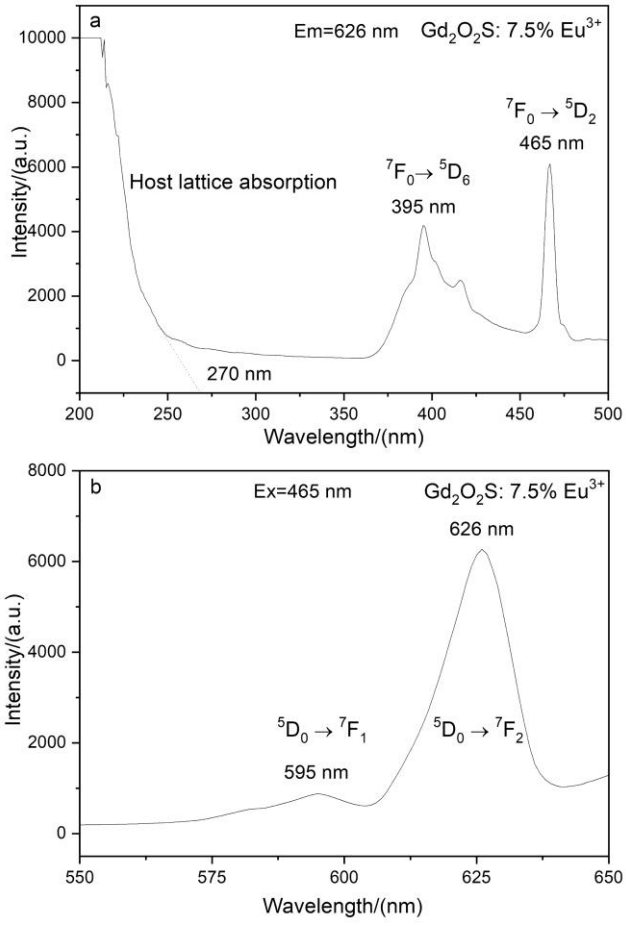

Fig. 11. (a) The excitation spectrum and (b) the emission spectrum of Gd_2O_2S:7.5% Eu^{3+} hollow spheres

To make sure the maximum Eu^{3+} doped concentration in $Gd_2O_2S:x\%Eu^{3+}$ host lattice, a series of Eu^{3+} doped phosphors were prepared. Fig. 12 shows the curve of the influence of the concentration of Eu^{3+} on the luminescent intensity of $Gd_2O_2S:x\%Eu^{3+}$. When the concentration of Eu^{3+} is between 1.25% and 7.50%, the photoluminescent intensity of $Gd_2O_2S:x\%Eu^{3+}$ increases gradually, especially when the concentration of Eu^{3+} is between 2.50% and 3.75%, and when the concentration of Eu^{3+} is 7.50%, the photoluminescent intensity reaches the highest value. When the concentration of Eu^{3+} is higher than 7.50%, the potoluminescence intensity of $Gd_2O_2S:x\%Eu^{3+}$ decreases linearly, which may be due to alone with the increase of Eu^{3+} concentration, the distance between Eu^{3+} ions become smaller, resulting in the enhancement of the exchange interaction between ions and the increase of the non radiative transition probability, thus the decrease of the luminescence intensity. Therefore, the quenching concentration of Eu^{3+} ions is 7.50%. This is also the reason why the optimum doping concentration is 7.5% in this study.

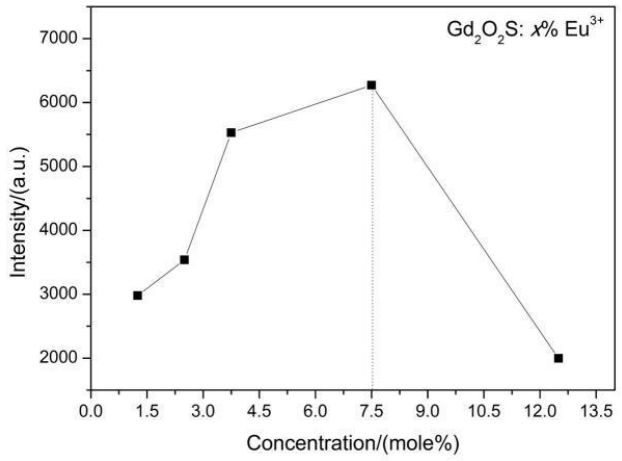

Fig. 12. Effect of Eu^{3+} doping concentration on the luminescence intensity of $Gd_2O_2S:x\%Eu^{3+}$ hollow spheres

To obtain the curve of the fluorescence lifetime of the target product $Gd_2O_2S:x\%\ Eu^{3+}$ (x=1.25, 2.50, 3.75, 7.50, 12.50) as revealed in Fig. 13. These curves accord with the following single-exponential decay behavior:

$$I_t=I_0\exp(-t/\tau) \quad (4)$$

where I_t is the intensity at time t, I_0 is the intensity at t=0, and τ is the decay lifetime. All the curves can be fitted by single exponential procedures. From Fig. 13, it can be seen that when the Eu^{3+} doping concentration is 1.25%, 2.50%, 3.75%, 7.50% and 12.50%, the fluorescence lifetimes are 0.111 μs, 0.111 μs, 0.111 μs, 0.114 μs and 0.111 μs, respectively.

According to the data, the fluorescence lifetimes of all $Gd_2O_2S:x\%Eu^{3+}$ with different Eu^{3+} doping concentrations are almost equal. When the Eu^{3+} doping concentration is 7.50%, the fluorescence lifetime is slightly longer, which may be related to the decrease of the defects, resulting in the reducing of the nonradiative pathways and suppressing of the luminescence quenching in the energy-transfer process.

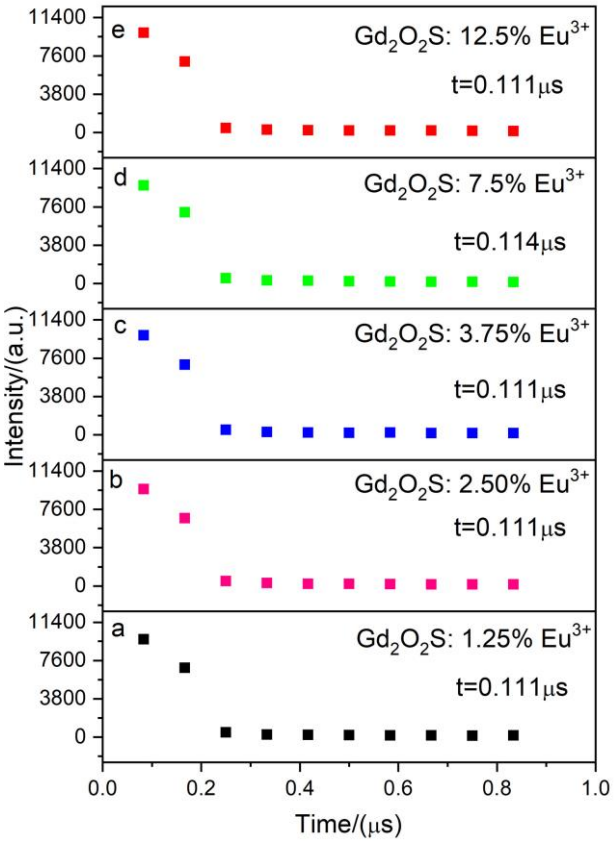

Fig. 13. Fluorescence lifetime fitting curve of $Gd_2O_2S:x\%Eu^{3+}$ hollow spheres (color online)

Generally, color can be represented by the Commission Inter-national de l'Eclairage (CIE) 1931 chromaticity coordinates. Here we employ the CIE chromaticity diagram to calculate the CIE chromaticity coordinate the of red emission and the results are shown in Fig. 14. Far and way, increasing the Eu^{3+} concentrations allows the colour to vary from a saffron to a orange colour. A linear increase in both the x and the y coordinates as a function of Eu^{3+} concentration is apparent. Table 1 shows the CIE coordinates of the phosphors with x% Eu^{3+} (x=1.25, 2.50, 3.75, 7.50, 12.50) are (0.576, 0.410), (0.585, 0.402), (0.618, 0.374), (0.629, 0.370) and (0.595, 0.394), respectively. As shown in Table 1, it can be seen that CIE x of the phosphor reaches the highest value when the doping concentration of Eu^{3+} ions is 7.50% in the study.

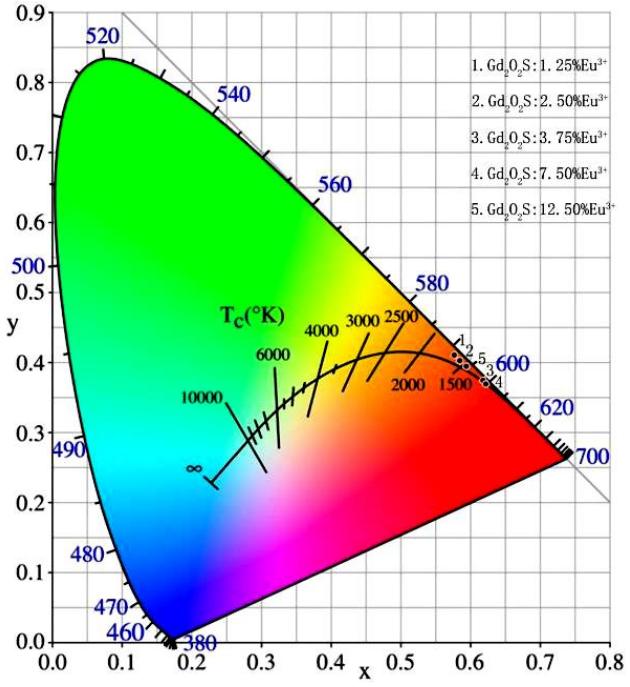

Fig. 14. CIE chromaticity coordinate diagram of $Gd_2O_2S:x\%\ Eu^{3+}$ hollow spheres (color online)

Table 1. CIE coordinates of $Gd_2O_2S:x\%\ Eu^{3+}$ hollow sphere

No.	CIE x	CIE y	Peak (nm)	Peak Intensity
1	0.576	0.410	626	2979
2	0.585	0.402	626	3538
3	0.618	0.374	626	5720
4	0.622	0.370	626	6271
5	0.595	0.394	626	3530

Table 2 shows the Summary and comparison between Gd_2O_2S:7.50% Eu^{3+} and Gd_2O_2S:7.0% Eu^{3+} from the following aspects: method, morphology/size, excitation /emission wavelength, intensity, lifetime and CIE coordinate. In their work, ethylenediamine was selected as the raw material. It's common knowledged that ethylenediamine will not only cause harm to human health but also unfriendly to the environment. Through the comparison of figures, the product obtained by our method in this work has a smoother surface and better dispersion with smaller size. From Table 2 we can also see clearly that the intensity of $Gd_2O_2S:Eu^{3+}$ hollow sphere by hydrothermal and reduction method is stronger. Under the excitation of 465 nm of blue light, it has a widespread application prospect compared with upon excitation at 260 nm. In this work, when the doping concentration of Eu^{3+} is 7.50%, its CIE coordinate fluorescence lifetime are (0.629, 0.370) and 1.114 μs. In summary, it's obviously that no matter in any aspect, the hollow sphere obtained by hydrothermal and reduction method has better comprehensive performance.

Table 2. Summary and comparison

Phosphor	Method	Morphology /Size	Excitation /Emission wavelength (nm)	Intensity	Lifetime (μs)	CIE coordinate (x,y)	Reference
Gd_2O_2S:7.50% Eu^{3+}	Hydrothermal /Reduction	Hollow sphere /200 nm	465/626	6271	0.1142	(0.629,0.370)	This work
Gd_2O_2S:7.0% Eu^{3+}	Solvothermal synthesis	Hollow sphere /2.5 μm	260/628	4213	497.3862	(0.586,0.302)	[16]

4. Conclusions

In this study, $Gd(NO_3)_3{\cdot}6H_2O$, $Eu(NO_3)_3{\cdot}6H_2O$, $NH_3{\cdot}H_2O$, L-cysteine and PVP were used as starting materials. The precursors were synthesized by hydrothermal method, and then the $Gd_2O_2S:Eu^{3+}$ hollow spheres were synthesized by calcination of the precursor and reduction of the $Gd_2O_2SO_4$, respectively. To sum up, the conclusions are demonstrated as follows: When PVP is 0.3 g and the hydrothermal reaction time is 12h, the precursor synthesized by hydrothermal reaction presents hollow sphere structure with wall thickness of about 50 nm, diameter of about 300-400 nm, uniform size and good dispersion. The precursor can be calcined in air for 800 °C for 2 h to obtain the $Gd_2O_2SO_4$, and the Gd_2O_2S can be obtained by calcing the $Gd_2O_2SO_4$ at 600 °C for 2 h in the reduction atmosphere and the Gd_2O_2S has hollow spherical structure, good dispersivity and particle size of

about 200 nm. The $Gd_2O_2S:Eu^{3+}$ hollow spheres can emit red light at 626 nm under the blue excitation of 465 nm, which is attributed to the $^5D_0 \rightarrow {}^7F_2$ transition of Eu^{3+} ions. The quenching concentration of $Gd_2O_2S:x\%Eu^{3+}$ is 7.50% and the corresponding fluorescence lifetime and CIE coordinates are τ = 1.114 μs and (0.629, 0.370), respectively. The study shows that hydrothermal assisted synthesis followed by reduction route reported in this paper is helpful for the synthesis of hollow spheres and the $Gd_2O_2S:Eu^{3+}$ hollow spheres may have potential applications in drug release and biomedical fields.

Acknowledgments

This work was supported by the Science and Technology Research Project of Department of Education of Liaoning Province (No. L2019021), Nature Science Foundation of Liaoning Province of China (No. 20170540582) and Fushun Revitalization Talents Program under Grant (No. FSYC202107011).

References

[1] J. Thirumalai, R. Chandramohan, T. A Vijayan, R. M. Somasundaram, Mater. Res. Bull. **46**, 285 (2011).
[2] L. Han, M. M. Pan, Y. Lv. Y. T. Gu, X. F. Wang, D. Li, Q. L. Kong, X. T. Dong, J. Mater. Sci.: Mater. Electron. **26**, 677 (2015).
[3] W. Wang, Y. Li, H. Kou, International Journal of Applied Ceramic Technology **12 S3**, E249 (2015).
[4] Y. Zhou, F. Li, X. J. Wang, Q. Zhu, X. D. Li, X. D. Sun, J. G. Li, Advanced Powder Technology **32**, 1911 (2021).
[5] X. Y. Huang, J. Y. Ding, X. Liu, X. Y. Li, H. H. Chen, D. J. Hu, D. Y. Zhu, T. F. Xie, J. R. Zhou, X. F. Jiang, Z. J. Sun, J. Li, Optical Materials **117**, 111192 (2021).
[6] C. Michail, I. Valais, I. Seferis, N. Kalyvas, S. David, G. Fountos, I. Kandarakis, Radiation Measurements **70**, 59 (2014).
[7] Z. G. Sun, B. Lu, G. P. Ren, H. B. Chen, Nanomaterials **10**, 1639 (2020).
[8] W. Wang, H. M. Kou, S. P. Liu, Y. Shi, J. Li, X. Q. Feng, Y. B. Pan, Y. S. Li, J. K. Guo, Ceram. Int. **41**, 2576 (2015).
[9] X. J. Peng, L. B. Nan, Q. Q. Tao, X. Z. Cheng, J. Z. Qiang, M. W. Jing, Materials Express **11**, 54 (2021).
[10] S. L. Gai, C. X. Li, P. P. Yang, J. Lin, Chem. Rev. **114**, 2343 (2014).
[11] S. X. Tong, X. G. Xi, L. J. Bao, W. N. Chu, Z. Xue, H. Jiao, Solid State Sciences **80**, 15 (2018).
[12] M. Kosari, A. Borgna, H. C. Zeng, ChemNanoMat **6**, 889 (2020).
[13] R. Li, L. Li, Y. Liang, N. Zhang, Y. Liu, S. Gan, Phys. Chem. Chem. Phys. **17**, 21485 (2015).
[14] A. M. El-Toni, M. A. Habila, J. P. Labis, Z. A. Alothman, M. Alhoshan, A. A. Elzatahryf, F. Zhang, Nanoscale **8**, 2510 (2016).
[15] X. X. Xua, B. Lu, J. X. Hua, Z. G. Sun, H. B. Chen, Journal of Luminescence **215**, 116702 (2019).
[16] P. Liaparinos, C. Michail, I. Valais, A. Karabotsos, I. Kandarakis, Applied Physics B-Lasers and Optics **128**, 76 (2022).
[17] H. Liu, F. Ye, H. B. Cao, G. Ji, J. Y. Lee, J. Yang, Nanoscale **5**, 6901(2013).
[18] J. Huang, Y. Song, Y. Sheng, K. Zheng, H. Li, H. Qi, X. Xue, Z. Hai, J. Alloy. Compd. **532**, 34 (2012).
[19] J. Xia, G. C. Li, Y. C. Mao, Y. Y. Li, P. K. Shen, L. P. Chen, CrystEngComm **14**, 4279 (2012).
[20] B. K. Kang, S. R. Mang, H. D. Lim, K. M. Song, Y. H. Song, D. H. Go, M. K. Jung, K. Senthil, D. H. Yoon, Materials Chemistry and Physics **147**, 178 (2014).
[21] G. Chen, F. S. Chen, X. H. Liu, W. Ma, H. M. Luo, J. H. Li, R. Z. Ma, G. Z. Qiu, Nano Research **7**, 1093 (2014).
[22] W. J. Bian, M. Zhou, G. Chen, X. Yua, M. Pokhrel, Y. B. Mao, H. M. Luo, Applied Materials Today **13**, 381 (2018).
[23] R. Manigandan, K. Giribabu, R. Suresh, S. Munusamy, S. Praveen Kumar, S. Muthamizh, T. Dhanasekaran, A. Padmanaban, V. Narayanan, Synthesis, RSC Adv. **5**, 7515 (2015).

*Corresponding author: lianjingbao@aliyun.com